Calculation of the O−H Stretching Vibrational Overtone Spectrum of the Water Dimer

Teemu Salmi,[†] Vesa Hänninen,[†] Anna L. Garden,[‡] Henrik G. Kjaergaard,[‡] Jonathan Tennyson,[§] and Lauri Halonen*[,†]

Laboratory of Physical Chemistry, P.O. Box 55 (A.I. Virtasen aukio 1), FIN-00014 University of Helsinki, Finland, Department of Chemistry, University of Otago, P.O. Box 56, 9054 Dunedin, New Zealand, and Department of Physics and Astronomy, University College London, Gower Street, London WC1E 6BT, United Kingdom

Received: January 25, 2008; Revised Manuscript Received: March 12, 2008

The O−H stretching vibrational overtone spectrum of the water dimer has been calculated with the dimer modeled as two individually vibrating monomer units. Vibrational term values and absorption intensities have been obtained variationally with a computed dipole moment surface and an internal coordinate Hamiltonian, which consists of exact kinetic energy operators within the Born−Oppenheimer approximation of the monomer units. Three-dimensional ab initio potential energy and dipole moment surfaces have been calculated using the internal coordinates of the monomer units using the coupled cluster method including single, double, and perturbative triple excitations [CCSD(T)] with the augmented correlation consistent valence triple ζ basis set (aug-cc-pVTZ). The augmented correlation consistent valence quadruple ζ basis set (aug-cc-pVQZ), counterpoise correction, basis set extrapolation to the complete basis set limit, relativistic corrections, and core and valence electron correlations effects have been included in one-dimensional potential energy surface cuts. The aim is both to investigate the level of ab initio and vibrational calculations necessary to produce accurate results when compared with experiment and to aid the detection of the water dimer under atmospheric conditions.

1. Introduction

The conversion of sunlight into heat in the Earth's atmosphere is due to absorption of light by atmospheric gases in distinct spectral regions and is therefore important in the Earth's energy balance. The broad absorption bands of ozone in the ultraviolet region are one well-known example because of their importance for biology on the Earth.[1] However, molecules that absorb infrared radiation emitted from the Earth's surface are more significant in the context of the greenhouse effect. These so-called greenhouse gases include the common molecules CO_2, CH_4, N_2O, O_3, and H_2O.

The role of water in the atmospheric energy balance is partly unknown. Two spectroscopically interesting processes include excess solar absorption[2–4] and so-called "water continuum" absorption.[5,6] In the former, the water dimer is assumed to play a role. In the latter, the absorption bands of water in the far-infrared region possess broad structures, the origin of which is under debate. One possible contribution to these bands arises from the low-frequency internal motions of water clusters, of which the water dimer is the simplest one.

The spectroscopy of water dimer has been studied extensively in the past. Several measurements of the water dimer spectra at nonequilibrium laboratory conditions have yielded a large amount of accurate information on the structure and energy levels.[7–17] Many of these studies have concentrated on the low-frequency vibrations but there is also some published work on the O−H stretching fundamentals and the first O−H stretching overtones.[15–19] Some earlier attempts to observe the water dimer in the atmosphere have failed,[2,20] but later there has been a reported observation in the high O−H stretching overtone region[21] although this result has been challenged.[22–24] However, recently, two laboratory measurements of the water continuum absorption near atmospheric sample conditions indicate the presence of the water dimer.[19,25]

The difference between the spectra of the water monomer and dimer arises from the hydrogen bond between the donor hydrogen atom and the acceptor oxygen atom. The vibrational energies associated with the O−H bond stretching that is located between the two oxygen atoms of the water dimer are lowered compared to stretching energies of the free water molecule. This difference is more pronounced at high O−H stretching energies, and it has been suggested that consequently the dimer and monomer spectra could be well-separated in certain regions.[26,27] For example, it has been proposed that observed absorption at 13 342 cm^{-1} is assigned as the third O−H stretching overtone of the dimer.[21] However, as mentioned, this assignment disagrees with other experiments where such absorption has not been observed.[28]

Computational studies can be used to estimate and predict water dimer vibrational energies. The water dimer possesses 12 vibrational degrees of freedom. At the moment, the full vibrational problem cannot be treated variationally to obtain converged eigenvalues for high-overtone states. However, the vibrations in the two water monomer units (denoted as an asymmetric donor and a symmetric acceptor) are weakly coupled to the large amplitude vibrations of the dimer. The interactions between high-frequency vibrations of different monomers are also weak.[29] Therefore, a simpler model can be used where the large amplitude vibrations are frozen such that the corresponding coordinates are constrained to the equilibrium values, and the coupling terms between the O−H stretching and the H−O−H bending vibrations of the different monomer units are excluded in the vibrational Hamiltonian.[26] Schofield and Kjaergaard[27] have used this approach to calculate the overtone spectra of the

* Corresponding author. E-mail: lauri.halonen@helsinki.fi.
[†] University of Helsinki.
[‡] University of Otago.
[§] University College London.

10.1021/jp800754y CCC: $40.75
Published on Web 06/21/2008

water dimer up to 20 000 cm^{-1}. Ab initio potential energy surfaces were computed using the quadratic configuration interaction electronic structure calculation method including single and double excitations and scaling to experimental water parameters. The vibrational eigenvalues for both the stretching and bending states were obtained with a harmonically coupled anharmonic oscillator (HCAO) model based on the use of curvilinear internal coordinates. These HCAO results are in reasonable agreement with the observations in refs 15−19. It is interesting that the HCAO result for the bonded O−H stretching third overtone is close (≈60 cm^{-1}) to the controversial observation at 13 342 cm^{-1}. The similarity of results obtained with a two-dimensional (2D)[26] and a three-dimensional (3D) HCAO[27] model suggests that the H−O−H bending modes have a limited effect on the high-frequency O−H stretching vibrational structure.

A curvilinear internal coordinate approach using exact kinetic energy operators within the Born−Oppenheimer approximation yields accurate results for small molecules when high-level ab initio methods are employed to calculate the potential energy surfaces.[30,31] For small molecules containing between three and six atoms, the fundamental vibrations calculated with high-level ab initio potential energy surfaces typically deviate only up to 10 cm^{-1} from experimental values. A better agreement can be obtained using more sophisticated electronic structure calculation models such as multireference configuration interaction,[32] high-order coupled cluster methods, and explicitly correlated R12 theory, which includes the interelectronic coordinate in the electronic wave function.[33] Deviations increase with higher excitation quantum number for the overtone states, and therefore, the best results are often achieved by optimizing some of the potential energy coefficients with the least-squares method using experimental vibrational term values as data.

In this work, we compute the overtone O−H stretching states of the water dimer using a model that treats the water dimer as two individually vibrating monomer units. The starting point is the HCAO model used previously.[26,27] We have employed, within the Born−Oppenheimer approximation, exact kinetic energy operators for the monomer units and calculated potential energy surfaces with the coupled cluster electronic structure calculation method, including single, double, and perturbative triple excitations [CCSD(T)]. Augmented correlation consistent valence triple- and quadruple-ζ basis sets (aug-cc-pVTZ and aug-cc-pVQZ) were used as basis functions. In addition, basis set extrapolation to the complete basis set (CBS) limit, core valence correlation corrections (CV), and second-order relativistic corrections were included to improve the energy. Absorption intensities have been computed using a dipole moment surface obtained with the CCSD(T) level of theory and the aug-cc-pVTZ basis set.

2. Theoretical Model

The vibration−rotation Hamiltonian of an N atomic molecule can be written as

$$H = T + V = -\frac{\hbar^2}{2}\sum_{\alpha}^{N}\frac{\nabla_\alpha^2}{m_\alpha} + V \qquad (1)$$

where the summation index α is over the nuclei, ∇_α is the gradient operator with respect to the position of the nucleus α, N is the number of nuclei, m_α is the mass of the αth nucleus, and V is the potential energy. By omitting the angular momentum components of the Hamiltonian, the kinetic energy T of the vibrational motion can be expressed as

$$T = -\frac{\hbar^2}{2}\sum_{ij}\left(\frac{\partial}{\partial q_i} + \frac{1}{J}\frac{\partial J}{\partial q_i}\right) g^{(q_i q_j)}\frac{\partial}{\partial q_j} \qquad (2)$$

where the summations are over the internal coordinates and the quantities

$$g^{(q_i q_j)} = \sum_{\alpha}^{N}\frac{1}{m_\alpha}(\nabla_\alpha q_i)\cdot(\nabla_\alpha q_j) \qquad (3)$$

are the elements of the mass-weighted reciprocal metric tensor, whose values are Wilson's g-matrix elements if evaluated at the reference position.[34] The volume element of integration is $d\tau = J dq_i dq_j ...$, where the weight function J is the Jacobian of the coordinate transformation. The kinetic energy is transformed into a form with a unit weight function.[35]

It is impractical to use an exact kinetic energy operator described above for all degrees of motion in the water dimer. The inclusion of the relative motions of monomers particularly causes complications in constructing an appropriate Hamiltonian operator. For example, the large amplitude acceptor tunneling motion, which possesses the lowest vibrational energy states of the water dimer, gives rise to kinetic energy terms that are theoretically unknown in the curvilinear internal coordinate representation. However, it is a good approximation to exclude the low-frequency motions from the model, because there is only a weak coupling between the low and high-frequency vibrations.[29] When the aim is to simulate O−H stretching overtone spectra, this simplifies the vibrational problem and makes variational calculations feasible. The O−H stretching and the H−O−H bending motions of the dimer are modeled using curvilinear internal bond coordinate Hamiltonian operators for the separate monomers. The kinetic energy terms are, within the Born−Oppenheimer approximation, exact operators for isolated bent triatomic molecules (see for example ref 36), and the potential energy terms are expressed in terms of the bond angle displacements $\Delta\theta = \theta - \theta_e$ and Morse variables $y = 1 - \exp(-a\Delta r)$, where a is the Morse steepness parameter, $\Delta r = r - r_e$, and r_e and θ_e are the equilibrium values of the bond lengths and the bond angles, respectively.[37,38]

The eigenvalues of the separate acceptor and donor Hamiltonians have been computed variationally using Morse oscillator and harmonic oscillator basis functions for the stretching and bending states, respectively. For the potential energy terms, known analytical expressions for integrals of the Morse and the harmonic oscillators were used in setting up Hamiltonian matrices.[38] Kinetic energy matrix elements were computed with Gauss−Hermite and Gauss−Laguerre numerical integrations.[39]

The infrared absorption intensities have been computed with an ab initio dipole moment surface combined with the lower and upper state eigenfunctions obtained by diagonalizing the Hamiltonian matrices. The use of Eckart axes would minimize vibration−rotation interactions[40–42] and should be used to obtain most accurate results. However, we have not transformed our surface to the Eckart frame because this transformation would likely have a small impact on the O−H stretching fundamentals and overtones of the water dimer.[43] We compute relative absorption intensities for transitions from the ground state g to an excited state e as follows[44]

$$f \propto \tilde{\nu}_{eg}\,|\vec{\mu}_{eg}|^2 \qquad (4)$$

where $\tilde{\nu}_{eg}$ is the transition wavenumber and $|\vec{\mu}_{eg}|^2$ is the square of the transition moment integral.

3. Ab Initio Calculations

The optimized geometries of the water dimer were calculated using coupled-cluster ab initio theory with single, double, and

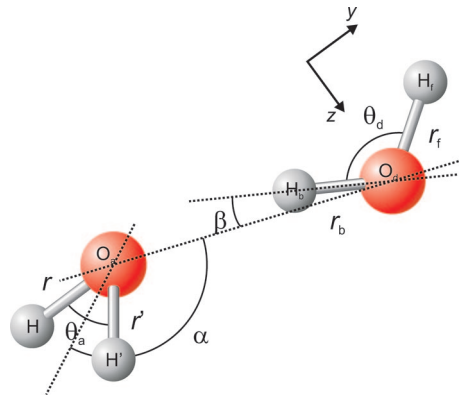

Figure 1. Coordinates of the water dimer.

TABLE 1: Geometric Parameters of Water Dimer[a]

	AVTZ	AVQZ	CP	CBS + CV + rel
		Acceptor		
r (Å)	0.9624	0.9597	0.9597	0.9574
θ_a (deg)	104.58	104.77	104.77	104.85
		Donor		
r_f (Å)	0.9608	0.9581	0.9581	0.9559
r_b (Å)	0.9678	0.9653	0.9651	0.9633
θ_d (deg)	104.53	104.71	104.70	104.77
		Monomer Positions		
r_{O-O} (Å)	2.9137	2.9095	2.9211	
α (deg)	121.85	123.05	123.57	
β (deg)	5.6444	5.6281	5.6326	

[a] 1 Å = 1 × 10^{-10} m.

perturbative triple excitations [CCSD(T)]. Correlation consistent aug-cc-pVTZ (AVTZ level) and aug-cc-pVQZ (AVQZ level) basis sets of Dunning and co-workers[45,46] were employed in these calculations. Unless otherwise stated, the frozen core approximation was used for the 1s electrons of the oxygen atoms. The geometry optimization was carried out using the quadratic steepest descent minimum search as implemented in the program MOLPRO,[47,48] which was used in all electronic structure calculations. It has been experimentally determined that the equilibrium structure of the water dimer belongs to the point group C_s such that the acceptor unit possesses local C_{2v} symmetry and the plane containing the donor unit bisects the bond angle of the acceptor unit.[49,50] Therefore, only 8 of 12 possible structural parameters were optimized. The definitions of the structural parameters are shown in Figure 1 and the optimized geometries are given in Table 1. These agree with previous calculations at similar ab initio levels.[29,51]

The anharmonic force fields including all three vibrational degrees of freedom were computed around optimized geometries for both of the monomeric units using the aug-cc-pVTZ basis set. The one-dimensional cuts of the potential energy surfaces (PES) were obtained by calculating eight single-point energies around the optimized geometry. The PES's were determined between −200 and +200 pm for the stretching coordinates and −20 and +20° for the bending coordinates around the equilibrium geometry.[26,27] The two-dimensional parts of the PES were calculated similarly by displacing two coordinates simultaneously. The surface was represented by a polynomial expansion in the bond angle displacements $\Delta\theta$ and in the Morse variables y. The coefficients of the series expansion were optimized with the least-squares method by using computed potential energy points as data. We improved this surface by computing the one-dimensional O−H stretching and H−O−H bending cuts with

TABLE 2: Water Dimer Potential Energy Surface Parameters[a]

	AVTZ	AVQZ	CP[b]	CBS + CV + rel	fit[c]
			Acceptor Unit		
a (Å^{-1})	1.9640	1.9552		1.7802	
T_2 (aJ)	1.0798	1.1008		1.3342	
T_3 (aJ)	−0.1769	−0.1953		−0.4055	
T_4 (aJ)	0.0945	0.0937		0.1409	
$f_{rr'}$ (aJ Å^{-2})	−0.1028				
$f_{rrr'}$ (aJ Å^{-3})	0.0095				
$f_{\theta\theta}$ (aJ)	0.7062	0.7052		0.7034	
$f_{\theta\theta\theta}$ (aJ)	−0.6716	−0.7024		−0.7200	
$f_{\theta\theta\theta\theta}$ (aJ)	−0.5762	−0.5897		−0.6230	
$f_{r\theta}$ (aJ Å^{-1})	0.2554				
$f_{r\theta\theta}$ (aJ Å^{-1})	−0.3304				
$f_{rr\theta}$ (aJ Å^{-2})	−0.1271				
$f_{rr\theta\theta}$ (aJ Å^{-2})	−0.1883				
			Donor Unit		
$a^{(f)}$ (Å^{-1})	1.9929	1.9495		1.8393	
$T_2^{(f)}$ (aJ)	1.0568	1.1161		1.2600	
$T_3^{(f)}$ (aJ)	−0.1602	−0.2077		−0.3338	
$T_4^{(f)}$ (aJ)	0.0873	0.0912		0.1149	
$a^{(b)}$ (Å^{-1})	2.3577	2.3780	2.3733	2.1909	2.2810
$T_2^{(b)}$ (aJ)	0.7075	0.7016	0.7062	0.8302	0.7915
$T_3^{(b)}$ (aJ)	0[d]	0[d]	0[d]	−0.0790	
$T_4^{(b)}$ (aJ)	0.0448	0.0433	0.0447	0.0329	
$T_6^{(b)}$ (aJ)	−0.0082	−0.0122	−0.0130	0[d]	
$f_{r_fr_b}$ (aJ Å^{-2})	−0.0902				
$f_{r_fr_br_b}$ (aJ Å^{-3})	0.0769				
$f_{r_fr_fr_b}$ (aJ Å^{-3})	−0.0391				
$f_{\theta\theta}$ (aJ)	0.7252	0.7234		0.7218	0.7188
$f_{\theta\theta\theta}$ (aJ)	−0.6522	−0.6851		−0.6951	
$f_{\theta\theta\theta\theta}$ (aJ)	−0.7011	−0.7028		−0.7290	
$f_{r_f\theta}$ (aJ Å^{-1})	0.2753				
$f_{r_f\theta\theta}$ (aJ Å^{-1})	−0.3103				
$f_{r_fr_f\theta}$ (aJ Å^{-2})	−0.1229				
$f_{r_fr_f\theta\theta}$ (aJ Å^{-2})	−0.1000				
$f_{r_b\theta}$ (aJ Å^{-1})	0.2043				
$f_{r_b\theta\theta}$ (aJ Å^{-1})	−0.2609				
$f_{r_br_b\theta}$ (aJ Å^{-2})	−0.3077				
$f_{r_br_b\theta\theta}$ (aJ Å^{-2})	0.0224				

[a] All angles are expressed in radians. [b] CP corrected PES slice with the AVQZ basis. [c] Apart from the values given, the parameters associated with one- and two-dimensional surface cuts were constrained to the CBS + CV + rel and AVTZ values, respectively. Evaluated at the CBS + CV + rel geometry from Table 1. [d] Constrained to zero.

the aug-cc-pVQZ basis set at the appropriate optimized geometry. The potential parameters obtained are given in Table 2, where the f parameters are the usual force constants (see refs 37 and 38 for the representation of the potential energy surface). The one-dimensional stretching surface cuts are defined as

$$V(y) = \sum_{i=1} T_i y^i \tag{5}$$

where the values of the T parameters (except T_1, which is constrained to zero) are given in Table 2.

The dipole surface needed for the intensity calculations was computed at the AVTZ level for both monomeric units of the water dimer. Each molecule-fixed axis component of the dipole surface was expressed in an analytic form as a Taylor series written as functions of the bond length and bond angle displacement coordinates. The coefficients of the series expansions were optimized with the linear-least-squares method using the computed dipole function points as data. The coefficients obtained are given in Table 3.

3.1. Potential Energy Corrections. The energy associated with the hydrogen bonding interaction in the water dimer is small when compared with orbital interactions. Therefore, we have taken basis set superposition error (BSSE) into account

TABLE 3: Dipole Function Expansion Coefficients for Water Dimer[a]

	x	y	z
Acceptor Unit			
μ_r (D Å^{-1})	−0.8700	− 0.3401	0.1406
μ_{rr} (D Å^{-2})	0.7616	0.2276	0.0135
μ_{rrr} (D Å^{-3})	4.2572	3.4847	−1.3377
$\mu_{r'}$ (D Å^{-1})	0.8700	−0.3401	0.1406
$\mu_{r'r'}$ (D Å^{-2})	−0.7616	0.2276	0.0135
$\mu_{r'r'r'}$ (D Å^{-3})	−4.2572	3.4847	−1.3377
μ_θ (D)		0.7406	−0.4107
$\mu_{\theta\theta}$ (D)		0.5326	−0.2267
$\mu_{\theta\theta\theta}$ (D)		0.5740	−0.2024
$\mu_{rr'}$ (D Å^{-2})		0.6805	−0.2289
$\mu_{rr'r'}$ (D Å^{-3})	−1.2384		−0.0249
$\mu_{rrr'}$ (D Å^{-3})	1.2384		−0.0249
$\mu_{r\theta}$ (D Å^{-1})	−1.2864	0.1630	−0.1356
$\mu_{r\theta\theta}$ (D Å^{-1})	−0.5899	0.1087	−0.1102
$\mu_{rr\theta}$ (D Å^{-2})	−0.0771	−0.1512	0.1095
$\mu_{rr\theta\theta}$ (D Å^{-2})	−1.1784	0.7224	−0.4088
$\mu_{r'\theta}$ (D Å^{-1})	1.2864	0.1630	−0.1356
$\mu_{r'\theta\theta}$ (D Å^{-1})	0.5899	0.1087	−0.1102
$\mu_{r'r'\theta}$ (D Å^{-2})	0.0771	−0.1512	0.1095
$\mu_{r'r'\theta\theta}$ (D Å^{-2})	1.1784	0.7224	−0.4088
Donor Unit			
μ_{r_f} (D Å^{-1})		0.6133	−0.1807
$\mu_{r_fr_f}$ (D Å^{-2})		−1.3197	0.4251
$\mu_{r_fr_fr_f}$ (D Å^{-3})		−4.4227	3.4819
μ_{r_b} (D Å^{-1})		−2.4766	−1.0994
$\mu_{r_br_b}$ (D Å^{-2})		−5.2628	−2.8167
$\mu_{r_br_br_b}$ (D Å^{-3})		−13.096	−5.6135
μ_θ (D)		−0.0577	0.6402
$\mu_{\theta\theta}$ (D)		0.3069	0.6474
$\mu_{\theta\theta\theta}$ (D)		0.4326	0.9644
$\mu_{r_fr_b}$ (D Å^{-2})		1.2484	0.1685
$\mu_{r_fr_br_b}$ (D Å^{-3})		0.7615	0.1356
$\mu_{r_fr_fr_b}$ (D Å^{-3})		−0.2607	−0.1883
$\mu_{r_fr_fr_br_b}$ (D Å^{-4})		1.5804	0.3825
$\mu_{r_f\theta}$ (D Å^{-1})		−1.9392	−0.3255
$\mu_{r_f\theta\theta}$ (D Å^{-1})		1.0462	0.6180
$\mu_{r_fr_f\theta}$ (D Å^{-2})		−2.7809	−1.7170
$\mu_{r_fr_f\theta\theta}$ (D Å^{-2})		6.2824	3.2954
$\mu_{r_b\theta}$ (D Å^{-1})		−0.3718	0.7390
$\mu_{r_b\theta\theta}$ (D Å^{-1})		0.2454	0.2908
$\mu_{r_br_b\theta}$ (D Å^{-2})		−1.6691	0.2650

[a] The x, y, and z axes are defined in Figure 1: 1 D is 3.33564×10^{-30} Cm. All angles are expressed in radians. The μ parameters are defined as derivatives of the dipole surface with respect to the internal coordinates.

using the most common approach, the counterpoise (CP) correction.[52] The CP corrected energy, $E^{(CP)}$ of the A−B dimer is defined as

$$E^{(CP)} = E_{AB}^{(AB)} + CP = E_{AB}^{(AB)} + (E_A^{(A)} - E_{AB}^{(A)}) + (E_B^{(B)} - E_{AB}^{(B)}) \quad (6)$$

where the superscripts refer to the system in question and subscripts to the basis used, i.e., for example, $E_{AB}^{(A)}$ is the energy of the monomer A calculated with the dimer basis set. We find the CP optimized geometry using the method described in ref 53, and the result is given in Table 1. In the case of the monomer unit potential energy surfaces, the largest BSSE correction is expected to be associated with the bonded hydrogen because it lies between the monomer units.[51] Therefore, we have improved the one-dimensional stretching PES of the bonded hydrogen using CP correction (eq 6) at the AVQZ level. The potential energy parameters are given in Table 2.

The single point energies at the complete basis set limit can be obtained using the equation[54]

$$E_X^{(HF)} = E_\infty^{(HF)} + ae^{-bX} \quad (7)$$

for the Hartree−Fock (HF) energy, and[55]

$$E_X^{(CORR)} = E_\infty^{(CORR)} + c/X^3 \quad (8)$$

for the correlation (CORR) energy. The quantity X represents the cardinal number of the basis set, a, b, and c are parameters, and $E_\infty^{(HF)}$ and $E_\infty^{(CORR)}$ are approriate energies at the complete basis set limit. The total energy at the complete basis set limit is

$$E_{CBS} = \lim_{X\to\infty}\left(E_X^{(HF)} + E_X^{(CORR)}\right) = E_\infty^{(HF)} + E_\infty^{(CORR)} \quad (9)$$

Thus, we need three HF and two correlation energies in order to calculate E_{CBS}. In this work, we have used aug-cc-pVXZ basis sets with the cardinal numbers $X = 3(T)$, 4(Q), and 5 for the HF energy, and 3(T) and 4(Q) for the correlation energy. These energies are calculated at the same geometries as the CP corrected AVQZ PES for the one-dimensional hydrogen bonded stretch and at the geometries of the AVQZ PES for the other one-dimensional stretches and one-dimensional bends using the same step sizes as earlier.

The core-valence (CV) and the relativistic corrections are also employed in order to further improve our PES. The CV correction is calculated by using the aug-cc-pCVTZ basis set[56] without the frozen core approximation, and the relativistic correction is computed at the aug-cc-pVTZ level using Douglas−Kroll one-electron integrals.[57] The magnitude of these corrections is calculated by subtracting the CCSD(T)/AVTZ energy from the corresponding corrected one.

The energy change in each of the aforementioned potential energy corrections is not a constant, i.e., its magnitude depends on geometry and therefore it changes the position of the potential energy minimum. In these one-dimensional problems, we have found the minimum by minimizing the coefficients of the T_1y and $f_\theta\Delta\theta$ potential energy terms. The structure obtained is given in Table 1, and the potential energy parameters are presented in Table 2.

4. Results and Discussion

It is obvious from Table 1 that the structures calculated with different methods are similar and in agreement with previous calculations and the experimantal structure. The eight structural parameters of the dimer have been optimized only at the AVTZ, AVQZ, and AVQZ + CP level of theory. The bond lengths in both monomer units decrease as the size of the basis set is increased from AVTZ to AVQZ. This leads to a steeper PES, which causes the vibrational energy levels to increase.[51] The inclusion of CP correction in the geometry optimization has little effect on the monomer unit geometries, but it alters the O−O bond length significantly.[51] As expected, the CP correction removes some artificial attraction between the monomers, and therefore the hydrogen bonding is weakened and the O−O bond length is increased.[51] In addition, as mentioned, BSSE affects the one-dimensional bonded O−H stretch and therefore the corresponding one-dimensional surface cut has been recalculated including the CP correction. A CP correction of the dipole moment function has been found to have a limited effect on the calculated intensities.[51]

There is no unique way to parametrize the potential energy surface, i.e. which sets of force constants are chosen. This was done by trial and error in different least-squares calculations

using ab initio energy points as data. Some additional potential energy points have been computed for the stretching vibrations in order to ensure the convergence of the fits. We have found that the best potential energy function of the three freely vibrating (non-hydrogen bonded) hydrogen atoms contains the terms T_2y^2, T_3y^3, and T_4y^4 in eq 5. The Morse steepness parameters a are optimized in addition to the T coefficients. The a parameters and the dissociation energy parameters T_2 assume somewhat unusual values although the ab initio potential energy points are well-presented by the chosen analytic representation of the potential energy surface. It was found that the stretching vibration of the bonded hydrogen was better represented by a potential model that includes the terms T_2y^2, T_4y^4, and T_6y^6. However, when the CBS, CV, and relativistic corrections were added, a slightly better fit to the ab initio points was obtained when instead of the T_6y^6 term the T_3y^3 term was included. The bending PES's are well-described by a fourth-order polynomial in the bond-angle displacement coordinates.

The variationally calculated vibrational energy levels of the water dimer together with computed absorption intensities for transitions starting from the ground vibrational state are presented in Table 4. The assignments have been obtained with the help of the eigenfunction expansions. The notation is such that we use the customary local mode quantum numbers for the acceptor.[59,60] We give the quantum labels (local mode labels) of the donor in the order: the free hydrogen stretch (H_f), the hydrogen-bonded hydrogen stretch (H_b), and the H_f–O–H_b bend.[27]

The energies of the bending modes agree well with the observed vibrational term values already at the AVTZ level. The AVQZ level bending energies are similar. Hence, it is not suprising that the additional small energy contributions to the one-dimensional bending potentials do not change this picture. Increasing the basis set raises the O−H stretching energy levels of both monomer units in agreement with previous calculations.[51] For the acceptor, our ab initio results agree well with the observations.[14–17,19] The bonded hydrogen stretch is the most interesting vibrational mode from the atmospheric observational point of view as the energies of the overtone vibrations may lie outside regions of strong water monomer absorption. Our CP corrected fundamental stretching energy ($|0\rangle_f|1\rangle_b|0\rangle$) is significantly lower (over 40 cm^{-1}) than the experimental value in ref 18. Our results for the other stretching fundamentals are closer to the experiment values, within 10 cm^{-1}.

To obtain better agreement with experiment in the case of the bonded hydrogen stretching mode, we employed a nonlinear least-squares method to optimize some of the model parameters using experimental vibrational term values as data (1614.7,[15] 3193.7, 5190.0, 5332.9, 6894.7, 7018.0 and 8821.1,[12] 3601 and 3735,[18] and 7240 cm^{-1} [17]). We obtained a better fit using the values from a matrix isolation study[12] for some states instead of the gas phase observations.[19] The ab initio values were used as the starting values for the optimized parameters, which in the case of the donor were the harmonic bending force constant $f_{\theta\theta}$, the harmonic wavenumber ω_b and the anharmonicity parameter ωx_b of the bonded hydrogen stretch (the harmonic wavenumber and the anharmonicity parameters can be computed from the Morse steepness parameters a and the parameters T_2, see ref 58). We also tried to optimize the parameters associated with the free O−H stretch, but they changed little, and the fitting did not improve the results. Therefore, ab initio values were used for these parameters. The standard deviation of the fit was 3.2 cm^{-1}. The optimization of some of the potential energy/spectroscopic parameters of the acceptor unit did not give any improvement when compared with the pure ab initio results. The potential energy parameters obtained from the least-squares calculation are given in Table 2. The harmonic bending force constant changes only slightly. The largest change occurs in the bonded O−H stretch. Both the harmonic wavenumber and the anharmonicity parameter increase. The net effect is such that vibrational energies increase. There are also significant changes in the energies of some other states. For instance, the wavenumber rises from 7223.1 to 7238.3 cm^{-1} for the state consisting mostly of $|2\rangle_f|0\rangle_b|0\rangle$. The reason for this behavior is the change in the mixing ratio of the free and bonded stretches. The assignment of the CBS + CV + rel energy level at 7223.1 cm^{-1} is 54% of $|2\rangle_f|0\rangle_b|0\rangle$ and 37% of $|1\rangle_f|1\rangle_b|0\rangle$, whereas the fitted one at 7237.4 cm^{-1} possesses more free character: 69% $|2\rangle_f|0\rangle_b|0\rangle$ and 23% $|1\rangle_f|1\rangle_b|0\rangle$. Similar behavior occurs in the $|3\rangle_f|0\rangle_b|0\rangle$ and $|3\rangle_f|1\rangle_b|0\rangle$ states.

There are some points worth mentioning concerning the details of the computed vibrational term values. The values of O−H stretching vibrational harmonic wavenumbers and the anharmonicity parameters in the donor unit are such that heavy mixing of the vibrational states occur at the first and higher stretching overtone manifolds. For example, although the $|0\rangle_f|2\rangle_b|0\rangle$ state is well-separated from the other pure stretching states (the state at the experimantal wavenumber 7018.0 cm^{-1} is 90% of $|0\rangle_f|2\rangle_b|0\rangle$), the assignment of the state at 7240 cm^{-1} is 37% of $|1\rangle_f|1\rangle_b|0\rangle$ and 54% of $|2\rangle_f|0\rangle_b|0\rangle$ and the state at 7362.0 cm^{-1} is 56% of $|1\rangle_f|1\rangle_b|0\rangle$ and 40% of $|2\rangle_f|0\rangle_b|0\rangle$ from the best ab initio calculation (CBS + CV + rel). These results depend strongly on the level of state mixing as can be seen from the corresponding numbers of the fitted surface 23 and 69% for the state at 7240 cm^{-1}, and 70 and 25% for the state at 7362.0 cm^{-1}. This mixing is one of the reasons assignment of experimental spectra of the first overtone region is so difficult.[17,29] The level of state mixing has been shown to vary significantly with ab initio method and vibrational model.[29] In the second overtone manifold, the pure stretching states $|1\rangle_f|2\rangle_b|0\rangle$, $|2\rangle_f|1\rangle_b|0\rangle$, and $|3\rangle_f|0\rangle_b|0\rangle$ are also heavily mixed. There is an additional complication at the second O−H stretching overtone manifold because the bonded hydrogen overtone state $|0\rangle_f|3\rangle_b|0\rangle$ is in a strong Fermi (cubic anharmonic) resonance[44] with a state involving bending character.[27] These kinds of mixings of the vibrational states become even more prominent at higher energies. The acceptor behaves more like the water monomer[38] because the pure stretching states contain little bending contribution until at high overtones.

The computed absorption intensities are worth some comments. In a system like the water dimer, the hydrogen stretching overtones and combinations are typically much stronger than transitions to states containing bending vibrational character. The acceptor unit is a local mode system (see refs 59–64 and references therein for the original work) where transitions to the local mode states $|m0\rangle^-|0\rangle$ and $|m0\rangle^+|0\rangle$ ($m > 0$) are stronger than transitions to the mixed states $|mn\rangle^-|0\rangle$ and $|mn\rangle^+|0\rangle$ (m, $n > 0$) within each overtone manifold ($m+n$ = constant). Generally, in the acceptor unit, the transitions to the antisymmetric states are stronger than to the corresponding symmetric states. In the donor unit, transitions to the local mode type states $|m\rangle_f|0\rangle_b|0\rangle$ and $|0\rangle_f|m\rangle_b|0\rangle$ are expected to be the strongest within each stretching vibrational overtone manifold. The bonded hydrogen stretching fundamental is the strongest band but at higher energies the free hydrogen stretching overtones become stronger than the bonded ones, due to a cancelation of terms in the transition dipole moment matrix element expansion for the bonded hydrogen stretch.[65] The mixing of the stretching states

TABLE 4: Calculated Energy Levels (cm^{-1}) and Relative Absorption Intensities for the Water Dimer[a]

						experiment		
local mode assignment	AVTZ	AVQZ[b]	CP[c]	CBS + CV + rel[b]	fit	matrix[d]	gas phase	intensities
$\|00\rangle^+\|1\rangle$	1594.8	1597.2		1597.4		1599.2	1600.6[e]	27.9
$\|0\rangle_f\|0\rangle_b\|1\rangle$	1616.3	1617.6	1617.9	1618.3	1614.5	1616.5	1614.7[e]	17.3
$\|00\rangle^+\|2\rangle$	3158.3	3161.2		3159.9		3163.0		0.21
$\|0\rangle_f\|0\rangle_b\|2\rangle$	3200.0	3200.9	3201.4	3201.2	3193.7	3193.7		1.8
$\|0\rangle_f\|1\rangle_b\|0\rangle(85\%)+\|1\rangle_f\|0\rangle_b\|0\rangle(13\%)$	3541.4	3554.3	3559.8	3558.7	3598.6	3590.5	3601[f]	100
$\|10\rangle^+\|0\rangle$	3631.0	3647.8		3654.2		3660.6	3660[g]	3.2
$\|1\rangle_f\|0\rangle_b\|0\rangle(85\%)+\|0\rangle_f\|1\rangle_b\|0\rangle(13\%)$	3709.7	3727.2	3727.7	3734.8	3739.4	3733.7	3735[f]	41.0
$\|10\rangle^-\|0\rangle$	3732.4	3750.0		3757.1		3750	3745.48[h]	22.6
$\|0\rangle_f\|1\rangle_b\|1\rangle(82\%)+\|1\rangle_f\|0\rangle_b\|1\rangle(12\%)$	5139.8	5153.9	5159.6	5158.6	5193.4	5190.0	5219[i]	0.85
$\|10\rangle^+\|1\rangle$	5205.2	5224.4		5230.7		5242.8		0.048
$\|10\rangle^-\|1\rangle$	5307.2	5327.7		5335.0		5328	5329[i]	2.7
$\|1\rangle_f\|0\rangle_b\|1\rangle(82\%)+\|0\rangle_f\|1\rangle_b\|1\rangle(13\%)$	5306.8	5325.9	5326.7	5334.2	5334.8	5332.9	5345[i]	1.1
$\|0\rangle_f\|1\rangle_b\|2\rangle$	6701.2	6714.8	6721.0	6718.8	6749.5			5.1×10^{-4}
$\|10\rangle^+\|2\rangle$	6746.9	6766.5		6771.1		6789.6		4.8×10^{-3}
$\|10\rangle^-\|2\rangle$	6851.2	6872.6		6878.6				0.050
$\|1\rangle_f\|0\rangle_b\|2\rangle$	6870.7	6889.9	6891.1	6897.9	6895.0	6894.7		0.014
$\|0\rangle_f\|2\rangle_b\|0\rangle$	6918.8	6940.7	6953.3	6947.4	7018.1	7018.0		0.10
$\|20\rangle^+\|0\rangle(75\%)+\|11\rangle^+\|0\rangle(17\%)$	7154.8	7186.3		7198.7		7206.6	7193[j]	0.26
$\|2\rangle_f\|0\rangle_b\|0\rangle(68\%)+\|1\rangle_f\|1\rangle_b\|0\rangle(23\%)$	7178.8	7210.1	7212.6	7223.1	7238.3	7237.1	7240[j]	0.30
$\|20\rangle^-\|0\rangle$	7204.8	7236.4		7249.4		7245	7249.8[j]	1.1
$\|1\rangle_f\|1\rangle_b\|0\rangle(69\%)+\|2\rangle_f\|0\rangle_b\|0\rangle(25\%)$	7304.8	7336.8	7340.6	7350.1	7380.0	7362.0		0.68
$\|11\rangle^+\|0\rangle(78\%)+\|20\rangle^+\|0\rangle(18\%)$	7400.8	7435.2		7449.0				5.9×10^{-3}
$\|0\rangle_f\|2\rangle_b\|1\rangle$	8501.0	8523.7	8536.7	8530.5	8594.4			4.7×10^{-3}
$\|20\rangle^+\|1\rangle(70\%)+\|11\rangle^+\|1\rangle(16\%)$	8708.9	8742.9		8754.9				1.2×10^{-3}
$\|20\rangle^-\|1\rangle$	8759.5	8793.9		8806.9				0.11
$\|2\rangle_f\|0\rangle_b\|1\rangle(63\%)+\|1\rangle_f\|1\rangle_b\|1\rangle(22\%)$	8759.0	8791.6	8794.4	8804.8	8815.7	8821.1		0.014
$\|1\rangle_f\|1\rangle_b\|1\rangle(66\%)+\|2\rangle_f\|0\rangle_b\|1\rangle(25\%)$	8882.1	8916.1	8920.3	8930.1	8955.3			3.8×10^{-3}
$\|11\rangle^+\|1\rangle(74\%)+\|20\rangle^+\|1\rangle(18\%)$	8955.4	8992.9		9006.9				9.7×10^{-6}
$\|0\rangle_f\|2\rangle_b\|2\rangle(69\%)+\|0\rangle_f\|3\rangle_b\|0\rangle(13\%)$	10027.7	10050.7	10065.6	10057.5	10120.2			5.3×10^{-4}
$\|0\rangle_f\|3\rangle_b\|0\rangle(80\%)+\|0\rangle_f\|2\rangle_b\|2\rangle(12\%)$	10125.9	10152.2	10171.9	10161.1	10241.0			3.9×10^{-3}
$\|30\rangle^+\|0\rangle(77\%)+\|21\rangle^+\|0\rangle(9\%)$	10538.2	10581.8		10601.0				3.7×10^{-3}
$\|3\rangle_f\|0\rangle_b\|0\rangle(67\%)+\|2\rangle_f\|1\rangle_b\|0\rangle(12\%)$	10550.7	10593.7	10599.0	10611.0	10633.5			0.013
$\|30\rangle^-\|0\rangle$	10552.1	10595.7		10615.3				0.036
$\|1\rangle_f\|2\rangle_b\|0\rangle(68\%)+\|3\rangle_f\|0\rangle_b\|0\rangle(15\%)$	10613.3	10655.9	10663.5	10673.7	10721.6			0.019
$\|21\rangle^+\|0\rangle(80\%)+\|30\rangle^+\|0\rangle(10\%)$	10802.9	10850.8		10869.7				1.6×10^{-3}
$\|2\rangle_f\|1\rangle_b\|0\rangle(74\%)+\|1\rangle_f\|2\rangle_b\|0\rangle(15\%)$	10824.4	10870.3	10876.8	10889.1	10933.5			7.0×10^{-3}
$\|21\rangle^-\|0\rangle$	10972.3	11021.8		11042.0				4.5×10^{-3}
$\|0\rangle_f\|4\rangle_b\|0\rangle$	13096.6	13124.4	13153.3	13139.2	13217.7		13342[k]	8.4×10^{-4}
$\|40\rangle^+\|0\rangle(72\%)+\|50\rangle^+\|0\rangle(10\%)$	13755.6	13808.9		13837.1				1.2×10^{-5}
$\|40\rangle^-\|0\rangle(73\%)+\|50\rangle^-\|0\rangle(10\%)$	13758.5	13811.8		13840.2				1.7×10^{-3}
$\|4\rangle_f\|0\rangle_b\|0\rangle$	13777.1	13824.2	13839.5	13841.8	13879.2			1.2×10^{-3}
$\|1\rangle_f\|3\rangle_b\|0\rangle$	13800.6	13855.7	13860.5	13882.5	13925.4			4.0×10^{-4}
$\|3\rangle_f\|1\rangle_b\|0\rangle(43\%)+\|2\rangle_f\|2\rangle_b\|0\rangle(32\%)$	14066.0	14121.9	14131.6	14144.2	14199.2			5.9×10^{-4}
$\|31\rangle^+\|0\rangle(55\%)+\|22\rangle^+\|0\rangle(22\%)$	14139.2	14199.3		14223.7				1.8×10^{-4}
$\|2\rangle_f\|2\rangle_b\|0\rangle(50\%)+\|3\rangle_f\|1\rangle_b\|0\rangle(38\%)$	14242.0	14299.9	14309.9	14324.0	14381.2			6.7×10^{-5}
$\|31\rangle^-\|0\rangle$	14240.6	14301.3		14327.5				3.0×10^{-4}
$\|22\rangle^+\|0\rangle(64\%)+\|31\rangle^+\|0\rangle(27\%)$	14463.7	14527.1		14553.6				2.6×10^{-6}
$\|0\rangle_f\|5\rangle_b\|0\rangle$	15911.4	15938.7	15978.9	15966.0	16028.5			2.6×10^{-4}
$\|50\rangle^+\|0\rangle(54\%)+\|60\rangle^+\|0\rangle(14\%)$	16821.9	16882.3		16920.4				1.1×10^{-5}
$\|50\rangle^-\|0\rangle(54\%)+\|60\rangle^-\|0\rangle(14\%)$	16822.5	16882.9		16921.1				7.4×10^{-5}

[a] The assignments and intensities are taken from the CBS + CV + rel calculation for the acceptor unit and from the fit for the donor unit. The intensities are scaled so that the value of 100 was attached to the strongest $|0\rangle_f|1\rangle_b|0\rangle$ band. [b] The two-dimensional surface part from the AVTZ surface (see Table 2). [c] PES as with AVQZ with the exception that four nonzero parameters were taken from Table 2 under heading CP. [d] Ne matrix values from ref 12. [e] From ref 15. For the state $|0\rangle_f|0\rangle_b|1\rangle$, alternative locations at 1613.8 and 1628.6 cm^{-1}. [f] From ref 18. [g] From ref 14. [h] From ref 16. [i] From ref 19, broad bands, large uncertainty. [j] From ref 17. [k] From ref 21.

from the first overtone manifold onward makes the transitions to the combinations states $|m\rangle_f|n\rangle_b|0\rangle$ ($m, n > 0$) stronger than is typical.

We may compare our results with the CC-VSCF calculations presented in ref 17 and the results obtained with the HCAO model including the H–O–H bending vibrations.[27] Our results are in better agreement with the HCAO model. For example, our computed band centers and relative intensities of the transitions to the stretching states $|20\rangle^-|0\rangle$, $|2\rangle_f|0\rangle_b|0\rangle$, $|20\rangle^+|0\rangle$, and $|1\rangle_f|1\rangle_b|0\rangle$ agree best with the results of ref 27 (HCAO). In this context, note that the states $|2\rangle_f|0\rangle_b|0\rangle$ and $|1\rangle_f|1\rangle_b|0\rangle$ are heavily mixed as mentioned earlier. The comparison with a high-resolution absorption experiment is interesting. As is seen from Table 4, we have assigned the water dimer bands at 7193, 7240, and 7249.8 cm^{-1}. We can also reproduce the observed relative intensities correctly. The band at 7249.8 cm^{-1} is the strongest and the bands at 7193 and 7240 cm^{-1} are about equally intense. The only experimental band we are unable to assign is the very weak feature at 7282 cm^{-1}, because it is too far away from our computed vibrational term values.

Band contour simulations give additional information on the assignments in the first O−H stretching region. The bands are

either a/c hybrids or pure b type structures.[16] The labeling is such that the inertial *a* axis is approximately along the O−O axis and the *c* axis is in the plane containing the donor atoms. The b and c type bands are characterized by somewhat widely spaced Q branches ($\Delta J = J' - J'' = 0$, where J is the total angular momentum quantum number, and the prime and the double prime refer to the upper and lower states, respectively). At low temperatures the a type band consists of strong R ($\Delta J = +1$) and P ($\Delta J = -1$) type transitions. The band at 7193 cm^{-1} looks like an a type band,[17] which is consistent with the assignment being $|20\rangle^{+}|0\rangle$. The band at 7249.8 cm^{-1} is assigned as $|20\rangle^{-}|0\rangle$ and thus it should possess a/b type structure. Looking at Figure 4 in ref 17, this is possible although the band shape is poorly defined. The band at 7240 cm^{-1} should be an a/c hybrid if the assignment $|2\rangle_f|0\rangle_b|0\rangle/|1\rangle_f|1\rangle_b|0\rangle$ is correct; again, the observed band shape is poorly defined.[17]

We have also performed similar calculations for the vibrational energies of the water monomer to obtain additional indications of how good the results are for the water dimer with the ab initio methods we have used. It is known that to obtain state-of-the-art results for the water monomer more sophisticated electronic structure calculations including multireference configuration interactions, nonadiabatic corrections due to the failure of the Born−Oppenheimer appromixations etc. are needed.[32] However, currently these advanced methods are computationally too expensive for the water dimer, and consequently we have restricted the ab initio computations to a more modest level. The number of points and grid sizes of the potential energy surface calculations and the analytic surface representation of the water monomer are identical to those used in the water dimer acceptor unit. For this work, the appropriate results of the variational vibrational calculations of the monomer are in Table 5. Comparing with experimental vibrational term values,[38,66] which are also given in Table 5, significant improvement occurs when the basis set size of the ab initio calculation is increased from AVTZ to AVQZ. The inclusion of basis set extrapolation to the complete basis set limit, relativistic corrections, and core-valence electron correlations effects do not change the overall agreement with experimental values. The water monomer results can be compared with the water dimer acceptor unit calculations where the hydrogen bonding plays a minor role when compared with the donor unit. In any case, the results indicate that, taking into account the uncertainty in the current experimental vibrational term values, it is possible to obtain good results for the water dimer using the chosen computational methods.

TABLE 5: Observed Energy Levels and Calculated Minus Observed Values in cm^{-1} at the Different Levels of Theory for the Water Monomer

	calculated[a]			
local mode assignment	AVTZ	AVQZ	CBS + CV + rel	observed[b]
$\|00\rangle^{+}\|1\rangle$	−1.7	0.7	1.2	1594.8
$\|00\rangle^{+}\|2\rangle$	2.5	5.3	4.7	3151.6
$\|10\rangle^{+}\|0\rangle$	−22.5	−5.6	1.3	3657.1
$\|10\rangle^{-}\|0\rangle$	−17.2	0.5	8.0	3755.9
$\|10\rangle^{+}\|1\rangle$	−27.4	−8.2	−1.0	5235.0
$\|10\rangle^{-}\|1\rangle$	−18.6	1.9	9.9	5331.3
$\|10\rangle^{+}\|2\rangle$	−27.8	−8.2	−2.3	6775.1
$\|10\rangle^{-}\|2\rangle$	−16.4	4.9	12.1	6871.5
$\|20\rangle^{+}\|0\rangle$	−40.7	−8.9	4.1	7201.5
$\|20\rangle^{-}\|0\rangle$	−37.4	−5.4	8.0	7249.8
$\|11\rangle^{+}\|0\rangle$	−33.7	0.9	15.4	7445.1
$\|20\rangle^{+}\|1\rangle$	−47.4	−13.2	−0.1	8761.6
$\|20\rangle^{-}\|1\rangle$	−40.2	−5.6	8.2	8807.0
$\|11\rangle^{+}\|1\rangle$	−34.2	3.4	18.5	9000.1
$\|30\rangle^{+}\|0\rangle$	−54.4	−10.4	8.8	10599.7
$\|30\rangle^{-}\|0\rangle$	−53.6	−9.6	10.0	10613.4
$\|21\rangle^{+}\|0\rangle$	−56.3	−8.0	11.8	10868.9
$\|21\rangle^{-}\|0\rangle$	−46.7	3.2	24.1	11032.4
$\|40\rangle^{+}\|0\rangle$	−66.8	−12.9	13.8	13828.3
$\|40\rangle^{-}\|0\rangle$	−66.3	−12.4	14.3	13830.9
$\|31\rangle^{+}\|0\rangle$	−73.6	−13.0	12.2	14221.1
$\|31\rangle^{-}\|0\rangle$	−67.2	−6.0	20.5	14318.8
$\|22\rangle^{+}\|0\rangle$	−58.9	5.0	32.1	14536.9
$\|50\rangle^{+}\|0\rangle$	−73.7	−12.7	21.5	16898.4
$\|50\rangle^{-}\|0\rangle$	−73.4	−12.4	21.7	16898.8

[a] Calculated with the CCSD(T) method as for the dimer in Table 4. [b] Observed wavenumbers are taken from refs 38 and 66, where the references to the original work can be found.

5. Conclusions and Summary

We have used a simple vibrational model to compute O−H stretching vibrational overtone spectra of the water dimer. We have included only the high-frequency modes of the acceptor and donor units in the model but the low-frequency modes are indirectly included in the sense that the potential energy surface contains their effects. The model allows us to test the current state-of-the-art quantum chemistry methods for water dimer including the size of the basis set, core−valence electron correlation, and relativistic corrections.

The model reproduces the observed O−H stretching and H−O−H bending vibrational terms values well. The largest differences occur in the hydrogen bonded O−H stretch, where, for example, in the case of the fundamental vibration, the difference is about 40 cm^{-1}. It is possible that a vibrational model that includes all or some of the low-frequency modes is needed for more accurate results for the bonded O−H stretch. The dependence of the harmonic wavenumber of the O−H stretch on the O−O stretching coordinate was found to have little effect on fundamental O−H vibrations.[67] However, the effect of the other low-frequency vibrations on the O−H stretching harmonic wavenumber has not yet been studied. We have investigated the bilinear kinetic and potential energy couplings (harmonic couplings) of some of the low-frequency modes with the hydrogen bonded O−H stretch using second order Van Vleck perturbation theory.[68,69] We have found that contributions to the harmonic wavenumber of the O−H stretch are small in magnitude. For example, the O−O stretching contribution is only about 1 cm^{-1}. Moreover, adding harmonic coupling between the O−H stretching modes of the donor and acceptor units has a limited effect on the O−H stretching transitions.[29] Thus, these corrections do not explain the 40 cm^{-1} difference. In order to obtain better agreement between the vibrational model and the experiment, we have optimized the harmonic wavenumber and the anharmonicity parameters of the bonded O−H stretching vibration and the harmonic bending force constant of the donor unit with the nonlinear least-squares method using observed vibrational terms values as data. In this way, we have obtained a surface that reproduces all observations well.

We can provide assignments for appropriate experimental observations. Our work also confirms the earlier results of the simpler 3D HCAO model that includes the O−H stretching and H−O−H bending vibrations. Our computed vibrational intensities for the O−H stretching vibrational bands show similar features to the intensities of the HCAO model: the bonded O−H stretching fundamental band is the strongest but the free hydrogen overtones or the free hydrogen and bonded hydrogen combination bands of the donor unit are stronger that the corresponding bonded overtones. As usual the pure stretching

overtones of both the donor and acceptor units are stronger than the stretch−bend combination bands. Cubic anharmonic resonances (Fermi resonances) between stretching and bending states change this picture locally.

It is pleasing that a simple model that includes the low-frequency modes indirectly reproduces well the fundamental and overtone vibrational terms values of the high-frequency modes in the water dimer. Approaches that include all modes would not produce converged variational eigenvalues at high O−H stretching energies. We believe that our work gives the best predictions for those bands that are useful for the detections of the water dimer in the Earth's atmosphere.

Acknowledgment. We thank Professor Poul Jørgensen from Aarhus University for helpful discussions. We thank the Academy of Finland, the University of Helsinki, the Marsden Fund administered by the Royal Society of New Zealand, and the QUASAAR EU-funded network for financial support. We also thank the CSC Scientific Computing Ltd. for providing computing time. Halonen is grateful to the Royal Society of London for funding during sabbatical leave in London. Kjaergaard thanks the Research Foundation at Aarhus University for a visiting professorship.

References and Notes

(1) Barry, R. G.; Chorley, R. J. *Atmosphere, Weather & Climate*, 7th ed; Routledge: London, 1998.
(2) Daniel, J. S.; Solomon, S.; Sanders, R. W.; Portman, R. W.; Miller, D. C.; Madsen, W. *J. Geophys. Res.* **1999**, *104*, 16785.
(3) Chylek, P.; Geldart, D. J.W. *Geophys. Res. Lett.* **1997**, *24*, 2015.
(4) Vaida, V.; Daniel, J. S.; Kjaergaard, H. G.; Goss, L. M.; Tuck, A. F. *Q. J. R. Meteorol. Soc.* **2001**, *127*, 1627.
(5) Cormier, J. G.; Hodges, J. T.; Drummond, J. R. *J. Chem. Phys.* **2005**, *122*, 114309.
(6) Sierk, B.; Solomon, S.; Daniel, J. S.; Portmann, R. W.; Gutman, S. I.; Langford, A. O.; Eubank, C. S.; Dutton, E. G.; Holub, K. H. *J. Geophys. Res.* **2004**, *109*, D08307.
(7) Burnham, C. J.; Xantheas, S. S.; Miller, M. A.; Applegate, B. E.; Miller, R. E. *J. Chem. Phys.* **2002**, *117*, 1109.
(8) Fröchtenicht, R.; Kaloudis, M.; Koch, M.; Huisken, F. *J. Chem. Phys.* **1996**, *105*, 6128.
(9) Fredin, L.; Nelander, B.; Ribbegard, G. *J. Chem. Phys.* **1977**, *66*, 4065.
(10) Perchard, J. P. *Chem. Phys.* **2001**, *266*, 109.
(11) Perchard, J. P. *Chem. Phys.* **2001**, *273*, 217.
(12) Boutellier, Y.; Perchard, J. P. *Chem. Phys.* **2004**, *305*, 1.
(13) Slipchenko, M. N.; Kuyanov, K. E.; Sartakov, B. G.; Vilesov, A. F. *J. Chem. Phys.* **2006**, *124*, 241101, and private communication.
(14) Buck, U.; Huisken, F. *Chem. Rev.* **2000**, *100*, 3863.
(15) Paul, J. B.; Provancal, R. A.; Chapo, C.; Roth, K.; Casaes, R.; Saykally, R. J. *J. Phys. Chem. A* **1999**, *103*, 2972.
(16) Huang, Z. S.; Miller, R. E. *J. Chem. Phys.* **1989**, *91*, 6613.
(17) Nizkorodov, S. A.; Ziemkiewicz, M.; Nesbitt, D. J. *J. Chem. Phys.* **2005**, *122*, 194316.
(18) Huisken, F.; Kaloudis, M.; Kulcke, A. *J. Chem. Phys.* **1996**, *104*, 17.
(19) Ptashnik, I. V.; Smith, K. M.; Shine, K. P.; Newnham, D. A. *Q. J. R. Meteorol. Soc.* **2004**, *130*, 2391.
(20) Hill, C.; Jones, R. L. *J. Geophys. Res.* **2000**, *105*, 9421.
(21) Pfeilsticker, K.; Lotter, A.; Peters, C.; Bösch, H. *Science* **2003**, *300*, 2078.
(22) Suhm, M. A. *Science (Lett.)* **2004**, *304*, 823.
(23) Pfeilsticker, K. *Science (Lett.)* **2004**, *304*, 824.
(24) Kassi, S.; Macko, P.; Naumenko, O.; Campargue, A. *Phys. Chem. Chem. Phys.* **2005**, *7*, 2460.
(25) Paynter, D.; Ptashnik, I.; Shine, K.; Smith, K. *Geophys. Res. Lett.* **2007**, *34*, L12808.
(26) Low, G. R.; Kjaergaard, H. G. *J. Chem. Phys.* **1999**, *110*, 9104.
(27) Schofield, D. P.; Kjaergaard, H. G. *Phys. Chem. Chem. Phys.* **2003**, *5*, 3100.
(28) Lotter, A. Field Measurements of Water Continuum and Water Dimer Absorption by Active Long Path Differential Optical Absorption Spectroscopy (DOAS), submitted to the combined Faculties for the Natural Sciences and for Mathematics of the Ruperto-Carola University of Heidelberg, Germany, for the degree of Doctor of Natural Sciences, examination date June 5, 2006.
(29) Kjaergaard H. G.; Garden, A. L.; Chaban, G. M.; Gerber, R. B.; Matthews, D. A.; Stanton, J. F. *J. Phys. Chem. A* **2008**, *112*, 4324.
(30) Rajamäki, T.; Noga, J.; Valiron, P.; Halonen, L. *Mol. Phys.* **2004**, *102*, 2259.
(31) Rajamäki, T.; Kallay, M.; Noga, J.; Valiron, P.; Halonen, L. *Mol. Phys.* **2004**, *102*, 2297.
(32) Polyansky, O. L.; Császár, A. G.; Shirin, S. V.; Zobov, N. F.; Barletta, P.; Tennyson, J.; Schwenke, D. W.; Knowles, P. J. *Science* **2003**, *299*, 539.
(33) Helgaker, T.; Jørgensen, P.; Olsen, J. *Molecular Electronic-Structure Theory*; John Wiley & Sons: New York, 2000.
(34) Wilson, E. B.; Decius, J. C.; Cross; P. C. *Molecular Vibrations*; Dover: New York, 1980.
(35) Pesonen, J.; Halonen, L. *Adv. Chem. Phys.* **2003**, *125*, 269.
(36) Wei, H.; Carrington, T., Jr. *J. Chem. Phys.* **1994**, *101*, 1343.
(37) Halonen, L.; Carrington, T., Jr. *J. Chem. Phys.* **1988**, *88*, 4171.
(38) Kauppi, E.; Halonen, L. *J. Phys. Chem.* **1990**, *94*, 5779.
(39) Stroud, A. H. *Gaussian Guadrature Formulas*; Prentice-Hall: Englewood Cliffs, N.J., 1966.
(40) Eckart, C. *Phys. Rev.* **1935**, *47*, 552.
(41) Le Sueur, C. R.; Miller, S.; Tennyson, J.; Sutcliffe, B. T. *Mol. Phys.* **1992**, *76*, 1147.
(42) Lawton, R. T.; Child, M. S. *Mol. Phys.* **1980**, *40*, 773.
(43) Kjaergaard, H. G.; Henry, B. R.; Wei, H.; Lefevre, S.; Carrington T, Jr.; Mortensen, O. S.; Sage, M. L. *J. Chem. Phys.* **1994**, *100*, 6228.
(44) Herzberg, G. *Molecular Spectra and Molecular Structure II. Infrared and Raman Spectroscopy of Polyatomic Molecules*; Van Nostrand Reinhold Company: New York, 1945.
(45) Kendall, R. A.; Dunning, T. H., Jr.; Harrison, R. J. *J. Chem. Phys.* **1992**, *96*, 6796.
(46) Dunning, T. H., Jr. *J. Chem. Phys.* **1989**, *90*, 1007.
(47) Werner, H.-J.; Knowles, P. J.; Lindh, R.; Manby, F. R.; Schütz, M.; Celani, P.; Korona, T.; Rauhut, G.; Amos, R. D.; Bernhardsson, A.; Berning, A.; Cooper, D. L.; Deegan, M. J. O.; Dobbyn, A. J.; Eckert, F.; Hampel, C.; Hetzer, G.; Lloyd, A. W.; McNicholas, S. J.; Meyer, W.; Mura, M. E.; Nicklass, A.; Palmieri, P.; Pitzer, R.; Schumann, U.; Stoll, H.; Stone, A. J.; Tarroni, R.; Thorsteinsson, T. MOLPRO, A Package of Ab Initio Programs, version 2002.6; http://www.molpro.net, 2002.
(48) Werner, H.-J.; Knowles, P. J.; Lindh, R.; Manby, F. R.; Schütz, M.; Celani, P.; Korona, T.; Rauhut, G.; Amos, R. D.; Bernhardsson, A.; Berning, A.; Cooper, D. L.; Deegan, M. J. O.; Dobbyn, A. J.; Eckert, F.; Hampel, C.; Hetzer, G.; Lloyd, A. W.; McNicholas, S. J.; Meyer, W.; Mura, M. E.; Nicklass, A.; Palmieri, P.; Pitzer, R.; Schumann, U.; Stoll, H.; Stone, A. J.; Tarroni, R.; Thorsteinsson, T. MOLPRO, A Package of Ab Initio Programs, version 2006.1; http://www.molpro.net, 2006.
(49) Klopper, W.; van Duijneveldt-van de Rijdt, J. G. C. M.; van Duijneveldt, F. B. *Phys. Chem. Chem. Phys.* **2000**, *2*, 2227.
(50) Dyke, T. R.; Mack, K. M.; Muenter, J. S. *J. Chem. Phys.* **1977**, *66*, 498.
(51) Schofield, D. P.; Lane, J. R.; Kjaergaard, H. G. *J. Phys. Chem. A* **2007**, *111*, 567.
(52) Boys, S. F.; Bernardi, F. *Mol. Phys.* **1970**, *19*, 553.
(53) Simon, S.; Duran, M.; Dannenberg, J. J. *J. Chem. Phys.* **1996**, *105*, 11024.
(54) Halkier, A.; Helgaker, T.; Jørgensen, P.; Klopper, W.; Olsen, J. *Phys. Lett.* **1999**, *302*, 437.
(55) Halkier, A.; Helgaker, T.; Jørgensen, P.; Klopper, W.; Koch, H.; Olsen, J.; Wilson, A. K. *Chem. Phys. Lett.* **1998**, *286*, 243.
(56) Woon, D. E.; Dunning, T. H. *J. Chem. Phys.* **1995**, *103*, 4572.
(57) de Jong, W. A.; Harrison, R. J. Dixon; D. A. *J. Chem. Phys.* **2001**, *114*, 48.
(58) Atkins, P. W. *Physical Chemistry*, 6th ed.; Oxford University Press: Oxford, U.K., 2001.
(59) Child, M. S.; Halonen, L. *Adv. Chem. Phys.* **1984**, *57*, 1.
(60) Halonen, L. *Adv. Chem. Phys.* **1998**, *104*, 41.
(61) Henry, B. R. *Acc. Chem. Res.* **1977**, *10*, 207.
(62) Sage, M. L.; Jortner, J. *Adv. Chem. Phys.* **1981**, *47*, 293.
(63) Child, M. S.; Lawton, R. T. *Faraday Discuss. Chem. Soc.* **1981**, *71*, 273.
(64) Mortensen, O. S.; Henry, B. R.; Mohammadi, M. A. *J. Chem. Phys.* **1981**, *75*, 4800.
(65) Kjaergaard, H. G.; Low, G. R.; Robinson, T. W.; Howard, D. L. *J. Phys. Chem. A* **2002**, *106*, 8955.
(66) Tennyson, J.; Zobov, N. F.; Williamson, R.; Polyansky, O. L.; Bernath, P. F. *J. Phys. Chem. Ref. Data* **2001**, *30*, 735.
(67) Garden, A. L.; Halonen, L.; Kjaergaard, H. G. *J. Phys. Chem. A*, accepted.
(68) Van Vleck, J. H. *Phys. Rev.* **1929**, *33*, 467.
(69) Kemble, E. C. *Fundamental Principles of Quantum Mechanics*; Dover: New York, 1958.

JP800754Y